Spectrochimica Acta Part A 92 (2012) 67–77

Contents lists available at SciVerse ScienceDirect

Spectrochimica Acta Part A: Molecular and Biomolecular Spectroscopy

journal homepage: www.elsevier.com/locate/saa

The spectroscopic (FTIR, FT-Raman, NMR and UV), first-order hyperpolarizability and HOMO–LUMO analysis of methylboronic acid

Usha Rani[a], M. Karabacak[b], O. Tanrıverdi[b], M. Kurt[c], N. Sundaraganesan[d,*]

[a] Research and Development Centre, Bharathiar University, Coimbatore 641046, India
[b] Department of Physics, AfyonKocatepe University, 03040 Afyonkarahisar, Turkey
[c] Department of Physics, Ahi Evran University, 40100 Kırsehir, Turkey
[d] Department of Physics (Engg.), Annamalai University, Annamalainagar 608 002, Tamil Nadu, India

ARTICLE INFO

Article history:
Received 2 November 2011
Received in revised form 2 February 2012
Accepted 10 February 2012

Keywords:
TD-DFT
Vibrational spectra
PES scan analysis
First order hyperpolarizability
Mulliken charges
Methylboronic acid

ABSTRACT

The solid phase FTIR and FT-Raman spectra of methylboronic acid (MBA) have been recorded in the regions 400–4000 and 50–4000 cm^{-1}, respectively. The spectra were interpreted interms of fundamentals modes, combination and overtone bands. The structure of the molecule was optimized and the structural characteristics were determined by density functional theory (B3LYP) and HF method with 6-311++G(d,p) as basis set. The vibrational frequencies were calculated for most stable conformer and were compared with the experimental frequencies, which yield good agreement between observed and calculated frequencies. The infrared and Raman spectra were also predicted from the calculated intensities. ^{1}H and ^{13}C NMR spectra were recorded and ^{1}H and ^{13}C nuclear magnetic resonance chemical shifts of the molecule were calculated using the gauge independent atomic orbital (GIAO) method. UV–visible spectrum of the compound was recorded in the region 200–400 nm and the electronic properties HOMO and LUMO energies were calculated by time-dependent TD-DFT approach. Mulliken charges of the MBA molecule was also calculated and interpreted. The geometric parameters, energies, harmonic vibrational frequencies, IR intensities, Raman intensities and absorption wavelengths were compared with the available experimental data of the molecule.

1. Introduction

Boron and boronic acid including organic compounds have been known for over a century. The boronic acid ligands have become an object of recent increasing interest due to their extensive applications in biology, crystal engineering, medicine, analytical chemistry and materials science. A wide variety of boronic acid derivatives of divergent biologically important compounds have been synthesized as anti-metabolites for a possible two-pronged attack on cancer [1–8]. Moreover to inhibition of tumor growth, the use of boron-10 neutron capture therapy [9] would be possible owing to the privileged localization of boron compounds in tumor texture. Boronic acid analogs for acyl transfer reactions [10] and inhibitors of dihydrotase [11]. The boronic acid moiety has also been associated into amino acid and nucleosides as anti-tumor, anti-viral agents [12].

Methylboronic acid $MeB(OH)_2$ (MBA) is the simplest of the mono organyl boranes. Methylboronic acid also exhibits a similar structural change on acid-base equilibrium [12]. Conformational analysis of methylboronic acid and its acyclic esters was studied by Valiakhmetova et al. [13]. Methylboronic acid and its acyclic esters were investigated by RHF/6-31G(d), MP2/6-31G(d), semi-empirical (AM1) and non-empirical quantum chemical approximations conformational isomerization. The experimental and theoretical vibrational spectra of 4-chloro- and 4-bromophenylboronic acid were studied by Kurt [14]. Horton et al. [15] investigated crystal structure of pentafluorophenylboronic acid molecule. Infrared and Raman spectra of 3,4-dicholorophenylboronic acid was studied by Kurt et al. [16] with density functional theory. Molecular structure, vibrational spectra and NBO analysis of 3,5-dicholorophenylboronic acid was investigated by Ayyappan et al. [17]. Alver and Parlak [18] investigated Infrared, Raman and NMR spectra of 2,6-dimethoxyphenylboronic acid using density functional theory.

In this work, we set out experimental and theoretical investigation of the conformation, vibrational and electronic transitions of methylboronic acid. The most stable conformers of MBA molecule have been studied within the framework DFT and HF. The geometric structure, vibrational wavenumbers, HOMO–LUMO energies and electric dipole moment of MBA have been studied. A detailed comment of the vibrational spectra of MBA has been made on the basis of the calculated total energy distribution (TED).

* Corresponding author. Tel.: +91 9442068405.
E-mail address: sundaraganesan_n2003@yahoo.co.in (N. Sundaraganesan).

1386-1425/$ – see front matter © 2012 Elsevier B.V. All rights reserved.
doi:10.1016/j.saa.2012.02.036

2. Experimental details

The Methylboronic acid sample was purchased from Sigma–Aldrich Chemical Company with a stated purity 97% and it was used as such without further purification. The sample was prepared using a KBr disc technique because of solid state. The FTIR spectrum of molecule was recorded in the region 400–4000 cm^{-1} on a Perkin Elmer FTIR BX spectrometer calibrated using polystyrene bands. FT-Raman spectrum of the sample was recorded using 1064 nm line of Nd:YAG laser as excitation wave length in the region 50–4000 cm^{-1} on a Bruker RFS 100/S FT-Raman spectrometer. The detector is a liquid nitrogen cooled Ge detector. Five hundred scans were accumulated at 4 cm^{-1} resolution using a laser power of 100 mW. The ultraviolet absorption spectra of MBA solved in ethanol are examined in the range 200–400 nm using Shimadzu UV-1800 PC, UV–vis recording Spectrometer. Data are analyzed by UV PC personal spectroscopy software, version 3.91. NMR experiments were performed in Bruker DPX 600 MHz at 300 K. The compound was dissolved in DMSO. Chemical shifts were reported in ppm relative to tetramethylsilane (TMS) for ^{1}H, ^{13}C NMR and DEPT 135 spectra. ^{1}H and ^{13}C NMR spectra were obtained at a base frequency of 600 MHz and 150 MHz, respectively.

3. Computational details

In order to obtain stable structures, the geometrical parameters including for three forms of MBA in the ground state (in vacuo) were optimized at DFT-B3LYP level of theory and ab initio-HF methods using 6-311++G(d,p) as basis set. There are no significant difference between geometric and vibrational frequencies by the selection of the different basis sets. The calculated vibrational frequencies are scaled by 0.9050 for HF [19]. For B3LYP with 6-311++G(d,p) basis set, the wavenumbers in the ranges from 4000 to 1700 cm^{-1} and lower than 1700 cm^{-1} are scaled with 0.958 and 0.983, respectively [20]. Total energy distribution (TED) calculations, which show the relative contributions of the redundant internal coordinates to each normal vibrational mode of the molecule, and thus enable us numerically to describe the character of each mode, were carried out by SQM method [21,22] using the output files created at the end of the frequency calculations. The B3LYP method allows calculating the shielding constants with accuracy and the GIAO method is one of the most common approaches for calculating nuclear magnetic shielding tensors. The ^{1}H and ^{13}C NMR isotropic shielding were calculated with the GIAO method [23,24] using the optimized parameters obtained from B3LYP/6-311++G(d,p) method. The theoretical results have enabled us to make the detailed assignments of the experimental IR and Raman spectra of the title molecule. All the calculations are performed by using Gauss view 5.0 molecular visualization program and Gaussian 09 program package on the personal computer [25].

4. Prediction of Raman intensities

The Raman activities (S_{Ra}) calculated with Gaussian 09 program [25] converted to relative Raman intensities (I_{Ra}) using the following relationship derived from the intensity theory of Raman scattering [26,27],

$$I_i = \frac{f(\nu_0 - \nu_i)^4 S_i}{\nu_i[1 - \exp(-hc\nu_i/kT)]}$$

where ν_0 is the laser exciting wavenumber in cm^{-1} (in this work, we have used the excitation wavenumber ν_0 = 9398.5 cm^{-1}, which corresponds to the wavelength of 1064 nm of a Nd:YAG laser), ν_i the vibrational wavenumber of the ith normal mode (cm^{-1}), while S_i is the Raman scattering activity of the normal mode ν_i. f (is a constant equal to 10^{-12}) is a suitably chosen common normalization factor for all peak intensities. h, k, c and T are Planck and Boltzmann constants, speed of light and temperature in Kelvin, respectively.

Table 1
The dipole moments μ (D) polarizability α, the average polarizability α_0, the anisotropy of the polarizability $\Delta\alpha$, and the first hyperpolarizability β ($\times 10^{-33}$ esu) of MBA, using B3LYP/6-311++G(d,p).

μ_x	−0.1169499	β_{xxx}	18.738340
μ_y	0.6091493	β_{xxy}	−3.582871
μ_z	0.0856664	β_{xyy}	−49.217921
μ_0	0.626162	β_{yyy}	19.887125
α_{xx}	37.012916	β_{xxz}	−10.704808
α_{xy}	−0.776383	β_{xyz}	1.476625
α_{yy}	37.427441	β_{yyz}	4.342349
α_{xz}	−3.406256	β_{xzz}	−2.201575
α_{yz}	0.645646	β_{yzz}	4.186070
α_{zz}	29.414029	β_{zzz}	21.998393
α_0	5.130407	β_x	−32.681156
$\Delta\alpha$	9.571165	β_y	20.490324
		β_z	15.635934
		β	359.58524

5. First order hyperpolarizability calculations

Polarizabilities and hyperpolarizabilities characterize the response of a system in an applied electric field [28]. They determine not only the strength of molecular interactions as well as the cross sections of different scattering and collision processes, but also the non-linear optical properties (NLO) of the system [29,30]. In order to investigate the relationships among photocurrent generation, molecular structures and NLO, the polarizabilities and hyperpolarizabilities of title compound was calculated using DFT-B3LYP method and 6-311++G(d,p) basis set, based on the finite-field approach. The first order hyperpolarizability (β) of MBA along with related properties (μ_0, α_0, and $\Delta\alpha$) are reported in Table 1. Because MBA has relatively homogeneous charge distribution it does not have large dipole moment. The calculated value of dipole moment was found to be 0.6261 Debye. The calculated anisotropy of the polarizability $\Delta\alpha$ of MBA is 9.5711×10^{-23} esu. The magnitude of the molecular hyperpolarizability β, is one of key factors in a NLO (non-linear optical) system. The B3LYP/6-311++G(d,p) calculated first order hyperpolarizability value (β) of MBA is equal to 0.3595×10^{-30} esu. Total dipole moment of title molecule is approximately two times smaller than those of urea and first order hyperpolarizability of title molecule is approximately equal to those of urea (μ and β of urea are 1.3732 Debye and 0.3728×10^{-30} esu obtained by HF/6-311G(d,p) method).

6. Results and discussion

6.1. Conformational analysis

On the basis of the definition of the standard conformer, theoretically, MBA molecule has three different possible conformers; the structures of all the conformers are shown in Fig. S1 (Supplementary data S1). The relative energies of the conformers calculated by B3LYP/6-311++G(d,p) method are collected in Table 2. Possible conformers of MBA depend on the rotation of C1–B3 bond, linked to boronic acid and methyl group. This bond is responsible for the flexibility and conformational stability of MBA. Thus, C1–B3–O4–H6 dihedral angle is a coordinate related to conformational flexibility. The MBA molecule has two fold rotation for the dihedral angle C1–B3–O4–H6; therefore, one can obtain a total of $2^2 = 4$ conformations. The potential energy surface (PES) of the dihedral angle C1–B3–O4–H6, calculated at the B3LYP level of theory, is displayed in Fig. 1. It seems that 2 conformers are located on PES graph. The internal rotational profile of C1–B3 bond was obtained

Table 2
Calculated energies and energy difference for three conformers of MBA by DFT.

Conformers	B3LYP6-311++G(d,p)		
	Energy (Hartree)	Energy (kcal mol^{-1})	Energy differences[a] (kcal mol^{-1})
Cis–Trans (ct)	−216.61363	−135927.10909	0.00000
Cis–Cis (cc)	−216.60943	−135924.47620	2.63289
Trans–Trans (tt)	−216.60886	−135924.11765	2.99144

[a] Energies of the other three conformers relative to the most stable ct conformer. *cis–trans* (ct) and *trans–cis* (tc) are the same conformers.

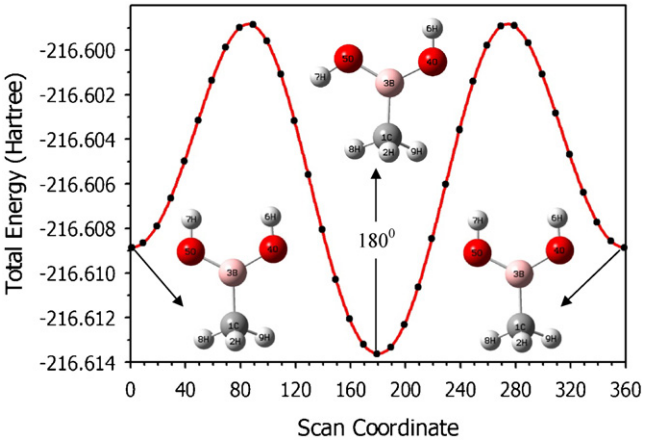

Fig. 1. PES scan for dihedral angle C1–B3–O4–H6 at B3LYP/6-311++G(d,p) method.

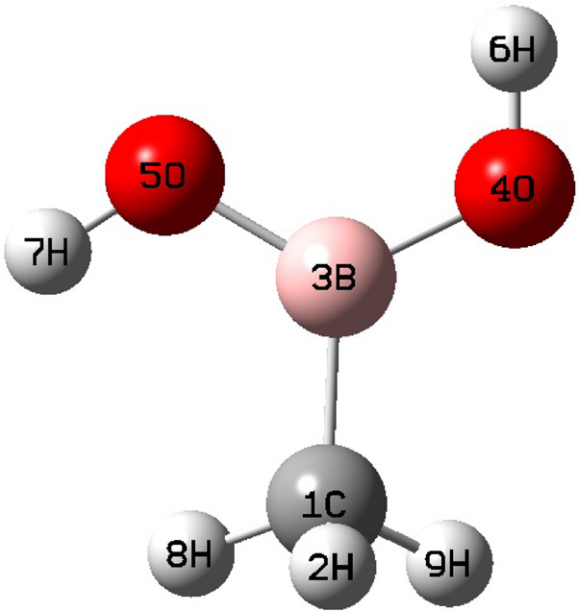

Fig. 2. Theoretical optimized possible geometric structure with atoms numbering of MBA (*cis–trans* form).

at B3LYP level of theory by allowing the torsional coordinate to vary in steps of 10° from 0° to 360°. This rotation bond yielded the energetically minima at 180°, with $E = -216.61362751$ Hartree for *cis–trans* conformer, and two higher energy minima at 0° and 360° for *cis–cis* conformer with $E = -216.60943173$ Hartree are shown on the potential energy curve of dihedral angle. It is evident that *cis–trans* conformer is the most stable form. The less stable conformer is *trans–trans* form (−216.60886034 Hartree), it is higher in energy than the conformational ground state. The main difference between the most stable and less stable conformers is 0.00476717 Hartree. The stability order for MBA conformers is *cis–trans* > *cis–cis* > *trans–trans* form. Therefore, in the present work we have focused on this form of MBA molecule to clarify molecular structure and assignment of vibrational spectra.

6.2. Spectroscopic properties

6.2.1. Structural analysis

The B3LYP/6-311++G(d,p) optimized structure of MBA molecule is shown in Fig. 2 and optimized bond lengths, bond angles, dihedral angles which were calculated by using B3LYP method are given in Table 3. The calculated geometrical parameters of all conformers along with available experimental data are presented in Table S2 (Supplementary data S2). In the present work, geometry

Table 3
The calculated geometric parameters of MBA for most stable conformer, bond lengths in angstrom (Å) and angles in degrees (°).

Bond lengths (Å)	X-ray[a]	X-ray[b]	HF	B3LYP	Dihedral Angles (°)	HF	B3LYP
B3–O4	1.362	1.355	1.354	1.366	H2–C1–B3–O4	96.3	97.0
B3–O5	1.378	1.362	1.364	1.378	H2–C1–B3–O5	−82.5	−81.8
C1–B3	1.568	1.579	1.579	1.573	H8–C1–B3–O4	−144.8	−144.0
O4–H6	0.750	0.920	0.942	0.964	H8–C1–B3–O5	36.3	37.2
O5–H7	0.750	0.820	0.940	0.960	H9–C1–B3–O4	−22.3	−21.6
C–$H_{average}$	–	–	1.087	1.095	H9–C1–B3–O5	158.9	159.6
Bond angles (°)					C1–B3–O4–H6	−178.3	−178.3
C1–B3–O4	118.8	118.2	119.8	119.6	O5–B3–O4–H6	0.6	0.6
C1–B3–O5	125.0	122.2	123.1	123.7	C1–B3–O5–H7	−1.5	−1.6
O4–B3–O5	–	119.5	117.0	116.7	O4–B3–O5–H7	179.7	179.6
B3–O4–H6	111.0	111.4	113.3	112.2			
B3–O5–H7	111.0	115.6	115.2	114.1			
B3–C1–H8	–	–	113.0	112.9			
B3–C1–H9	–	–	111.6	111.7			
B3–C1–H2	–	–	109.4	109.9			
H–C–$H_{average}$	–	–	107.6	107.4			

[a] Taken from Ref. [32].
[b] Taken from Ref. [33].

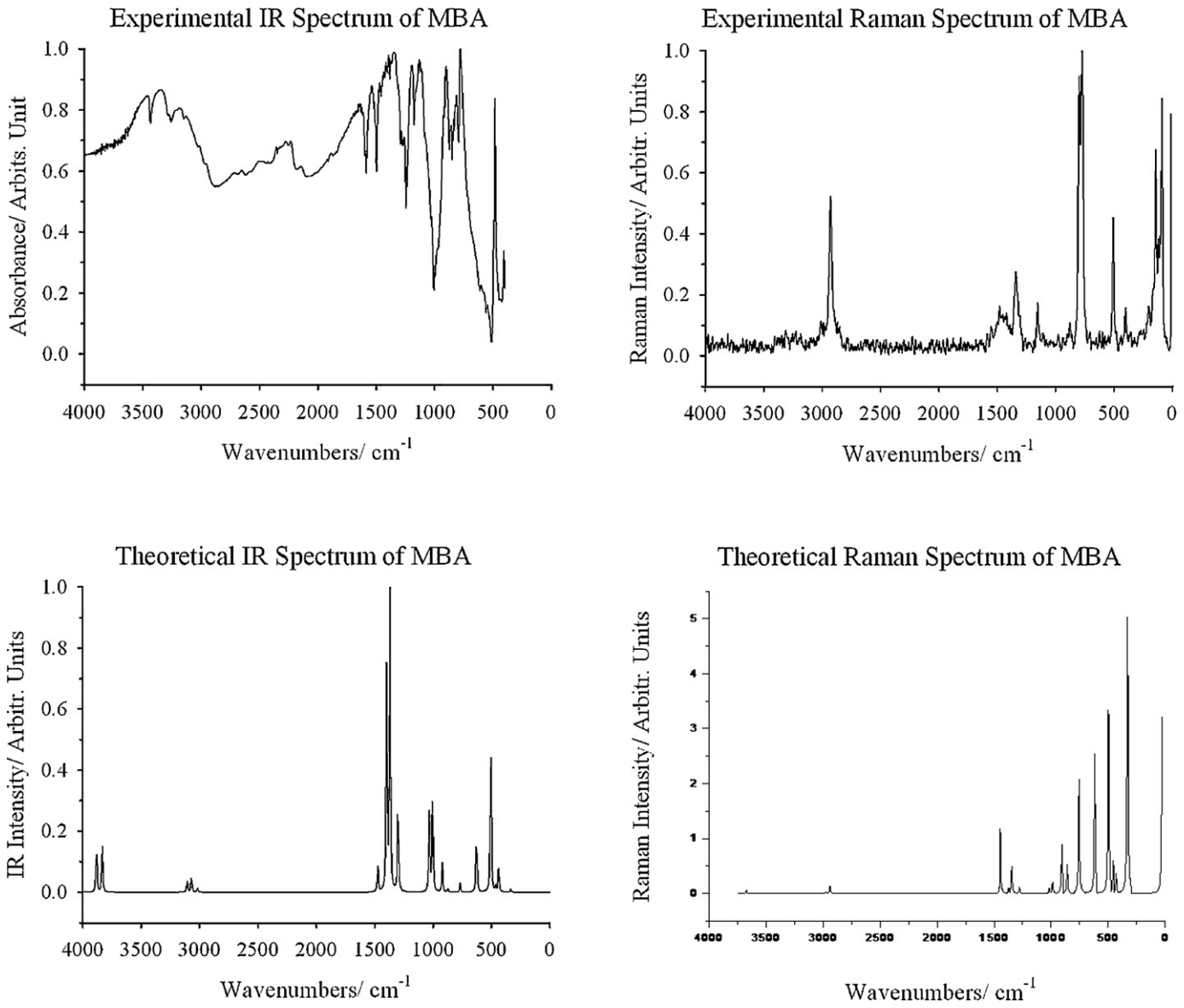

Fig. 3. Experimental and theoretical infrared and Raman spectra of MBA.

optimization of bond lengths, bond angles and dihedral angles for MBA has been employed without symmetry constrain. The equilibrium geometry has been determined by the energy minimization. This geometry optimization produced a molecular structure which is remarkably similar to one of the crystallographic asymmetric unit [31]. The increase in size of basis set gives rise to the bigger values in the orientation of dihedral angle due to its electron correlation approximation and polarization effect. The geometry of the molecule under investigation is considered by possessing C_s point group symmetry. The optimized parameter values were compared with the X-ray data of closely related molecules [15,32]. The optimized bond lengths and the bond angles are slightly different from the experimental values. We noted that the experimental results belong to the solid phase and theoretical calculations belong to the gas phase. In the solid state the experimental results are related to molecular packing, but in the gas phase the isolated molecules are considered in the theoretical calculations. The maximum difference between the experimental values and those obtained from the theoretical calculations is 0.214 Å for bond distances and 4.2° for bond angles. In general, typical B–O distances are 1.359 Å consistent with relatively strong π-interactions. In our title molecule, the B–O bond distances are in well agreement with the experimental data. Both the hydrogen atoms are in the O–B–O plane. Most probably, the oxygen lone pairs have a resonance interaction with the empty p orbital of boron, which forces the hydrogen to be in the O–B–O plane. However, in the lowest-energy form of MBA the $-B(OH)_2$ group is planar and, at all the computational levels, it does not lie in the plane of the methyl group. The O–B–O plane was twisted by ∼3.3° for the DFT method and by ∼3° for the HF method. It is evident from Table 3. Since the geometry of the molecule obtained by B3LYP/6-311++G(d,p) method is energetically most stable, hence the theoretical values of this method are taken for correlation and is more reliable.

6.2.2. *Vibrational spectra analysis*

The vibrational spectrum is mainly determined by the modes of the free molecule observed at higher wavenumbers, together with the lattice (translational and vibrational) modes in the low wavenumber region. In our present study, we have performed a frequency calculation analysis to obtain the spectroscopic signature of Methyl boronic acid. The MBA molecule consists of 9 atoms therefore they have 21 vibrational normal modes. All the frequencies

Table 4a
The observed FTIR, FT-Raman and calculated wavenumbers (in cm^{-1}) using B3LYP/6-311++G(d,p) along with their relative intensities ($km\,mol^{-1}$), scattering activities ($Å^4\,amu^{-1}$), and total energy distribution (TED) of MBA.

Mode nos.	Experimental		B3LYP/6-311++G(d,p)					Assignments based on TED (≥10%)
	FTIR	FT-Raman	Unscaled	Scaled	I_{IR}	S_{Ra}	I_{Ra}	
1			3883	3720	58.20	75.16	0.20	υO_5H_7 (100)
2	3424		3834	3673	50.79	119.14	1.12	υO_4H_6 (100)
3	3222		3107	2977	15.74	69.04	0.51	$υ_{asym}CH_3$ (97)
4	3086		3069	2940	18.23	65.58	2.88	$υ_{asym}CH_3$ (100)
5	2990	2930	3018	2892	4.99	158.05	0.07	$υ_{sym}CH_3$ (100)
	2189							Overtone/combination
	2107							Overtone/combination
	1582							Overtone/combination
6	1496	1486	1479	1453	5.21	4.91	2.73	ρ HCH (56) + Γ OBCH (21) + δ BCH (12)
7	1452		1473	1448	21.59	3.84	23.15	ρ HCH (50) + Γ OBCH (25) + δ BCH (11)
8	1402		1398	1374	251.39	1.65	1.89	υBO (34) + υBC (18) + ωHCH (14)
9	1380	1359	1370	1346	328.49	1.50	9.88	υBO (53) + δHCH (11) + δ BCH (10)
10	1244		1301	1279	110.48	0.67	2.21	δ HCH (30) + δ BCH (26) + υBO (19) + δ HOB (14)
11	1172	1187	1034	1016	82.66	2.25	1.97	δ O_4H_6 (79) + υBO (20)
12	1004		1005	988	135.87	3.55	4.03	δ O_5H_7 (70) + υBO (20)
13	916		921	906	30.08	0.15	17.60	rCH_3 (72) + Γ OBCH (20)
14	872		875	860	3.88	0.93	10.20	rCH_3 (61) + Γ OBCH (15)
15	792	793	769	756	1.35	9.98	40.34	υB-CH_3 (60) + υBO (33)
16	544		628	618	75.39	0.48	49.62	γ O_4H_6 (81) + Γ HOBO (10)
17	508	512	507	498	178.87	0.24	67.34	γ O_5H_7 (91)
18			464	456	5.07	0.56	11.78	γ HOBC (72) + γ HCB (15)
19	430		438	430	27.30	0.72	7.19	δ OBO (53) + δ OBC (27)
20		145	337	331	2.71	0.36	100.00	δ OBC (87)
21		95	28	27	0.13	0.29	64.54	Γ CH_3 (99)

I_{IR}, IR intensity; S_{Ra}, Raman scattering activity; I_{Ra}, Raman intensity; $υ_{sym}$, symmetric stretching; $υ_{asym}$, asymmetric stretching; δ, bending; γ, out-of-plane bending; ρ, scissoring; ω, wagging; r, rocking; Γ, torsion.
TED < 10% are not shown.

are assigned in terms of fundamental, overtone and combination bands. Assignments have been made on the basis of relative intensities, energies, line shape and total energy distribution (TED). The measured (FTIR and FT-Raman) wavenumbers and assigned wavenumbers of the some selected intense vibrational modes calculated at the HF and B3LYP level using basis set 6-311++G(d,p) along with their TED are given in Table 4. The calculated Raman and IR intensities were used to convolute each predicted vibrational mode with a Lorentzian line shape with a full width at half maximum (FWHM = 10 cm^{-1}) to produce simulated spectra. This reveals good correspondence between theory and experiment in main spectral features. The experimental and theoretical FTIR and FT-Raman spectra are shown in Fig. 3. The wavenumbers calculated at the HF level are higher than the ones from B3LYP. Inclusion of

Table 4b
The observed FTIR, FT-Raman and calculated wavenumbers (in cm^{-1}) using HF/6-311++G(d,p) along with their relative intensities ($km\,mol^{-1}$), scattering activities ($Å^4\,amu^{-1}$), and total energy distribution (TED) of MBA.

No	Experimental		HF/6-311++G(d,p)					Assignments based on TED (≥10%)
	FTIR	FT-Raman	Unscaled	Scaled	I_{IR}	S_{Ra}	I_{Ra}	
1			4218	4041	94.97	52.89	0.15	υO_5H_7 (100)
2	3424		4175	4000	98.13	79.85	0.84	υO_4H_6 (100)
3	3222		3240	3104	25.27	69.38	0.49	$υ_{asym}CH_3$ (100)
4	3086		3195	3061	33.27	66.67	2.80	$υ_{asym}CH_3$ (98)
5	2990	2930	3146	3014	8.63	152.81	0.06	$υ_{sym}CH_3$ (100)
	2189							Overtone/combination
	2107							Overtone/combination
	1582							Overtone/combination
6	1496	1486	1591	1564	4.59	5.73	2.54	ρ HCH (57) + Γ OBCH (29) + δ BCH (10)
7	1452		1582	1555	14.83	5.27	21.65	ρ HCH (53) + Γ OBCH (27) + δ BCH (10)
8	1402		1501	1476	247.89	1.33	1.77	υBO (34) + υBC (18) + ωHCH (14)
9	1380	1359	1462	1437	402.76	0.64	9.44	υBO (53) + δHCH (11) + δ BCH (10)
10	1244		1387	1364	194.37	0.52	2.12	υBO (24) + δHCH (23) + δBCH (20) + δHOB (19) + δHCH (11)
11	1172	1187	1108	1089	85.86	1.48	1.89	ρ HOB (80) + υBO (20)
12	1004		1077	1058	139.86	2.60	3.87	ρ HOB (68) + υ BO (20)
13	916		990	974	46.24	0.25	16.80	rCH_3 (51) + Γ OBCH (40)
14	872		942	926	3.80	1.27	9.69	rCH_3 (51) + Γ OBCH (14)
15	792	793	803	789	8.76	8.34	41.44	υB-CH_3 (60) + υBO (32)
16			651	640	110.80	0.31	52.04	γ O_4H_6 (79)
17	544		537	528	189.56	0.21	67.34	γ O_5H_7 (94)
18	508	512	493	485	10.42	0.63	11.72	γ HOBC (61) + γ HCB (13)
19	430		467	459	28.18	0.70	10.57	δ OBO (50) + δ OBC (25)
20		145	358	352	3.03	0.15	100.00	δ OBC (87)
21		95	37	37	0.11	0.18	54.95	Γ CH_3 (99)

I_{IR}, IR intensity; S_{Ra}, Raman scattering activity; I_{Ra}, Raman intensity; $υ_{sym}$, symmetric stretching; $υ_{asym}$, asymmetric stretching; δ, bending; γ, out-of-plane bending; ρ, scissoring; ω, wagging; r, rocking; Γ, torsion.
TED < 10% are not shown.

Table 5
Experimental and theoretical ^{1}H and ^{13}C isotropic chemical shifts (with respect to TMS) of MBA in DMSO and Gas phase (all values in ppm).

Atom	Experimental	Theoretical	
		DMSO	Gas
C1	−0.301	−0.248	0.604
H2	0.054	0.411	0.420
H6	7.425	4.799	3.354
H7	7.429	5.364	3.852
H8	0.054	−0.078	−0.342
H9	0.054	0.164	0.419

electron correlation in DFT to a certain extent makes the wavenumber values smaller in comparison to the HF wavenumber values.

6.2.2.1. O–H vibrations. In the O–H region, very strong and broad bands in the spectra of some boronic acid molecules occur at ca 3300 cm^{-1}. The assignment of these bands to O–H stretching vibrations is straightforward. The strength and broadening wavenumbers of these bands suggest that intramolecular hydrogen bonding occurs in different environments of boronic acids [33]. In accordance with the above conclusion, the O–H stretching vibration occurs at 3424 cm^{-1} in the FTIR spectrum. The theoretically predicted wavenumbers by the B3LYP and HF methods for the most stable *cis–trans* form show slightly on the higher side of wavenumbers at 3720, 3673 cm^{-1} and 4041, 4000 cm^{-1} respectively, which may be due to the presence of intramolecular hydrogen bonding. As expected, these two modes are pure stretching modes as evident from the TED column; they contribute exactly 100%. The observed values are in good agreement with the literature data [17].

The O–H in-plane bending vibrations, in general lies in the region 1150–1250 cm^{-1} and is not much affected due to hydrogen bonding unlike to stretching and out-of-plane bending frequencies [34]. The medium strong band in FTIR spectrum at 1172–1004 cm^{-1} is assigned to O–H in-plane bending vibration for both the O–H groups in the MBA molecule. The theoretically computed values at 1016 and 988 cm^{-1} by B3LYP/6-311++G(d,p) method show moderate agreement with recorded spectrum. The O–H out-of-plane bending vibrations are also calculated at 618, 498 cm^{-1} by B3LYP method and 640, 528 cm^{-1} by HF method (mode nos. 16 and 17).

6.2.2.2. Methyl group vibrations. The MBA molecule under consideration possesses one CH_3 unit which lies in the terminal group of molecule. For the assignments of CH_3 group frequencies, nine fundamentals can be associated to each CH_3 group [35]. The C–H stretching in CH_3 occurs at lower frequencies than those of aromatic ring (3100–3000 cm^{-1}). Moreover, the asymmetric stretch is usually at higher wavenumber than the symmetric stretch. Methyl group vibrations are generally referred to as electron-donating substituent in the aromatic rings system, the antisymmetric C–H stretching mode of CH_3 is expected around 2980 cm^{-1} and CH_3 symmetric stretching is expected at 2870 cm^{-1} [36,37]. The CH_3 asymmetric stretching vibration is calculated at 2977, 2940 cm^{-1} by B3LYP method and at 3104, 3061 cm^{-1} by HF method. The CH_3 symmetric stretching mode is predicted by B3LYP method at 2892 cm^{-1} and by HF method at 3014 cm^{-1}. These vibrations show more than 97% of TED contribution suggesting that it is a pure stretching mode. The same vibrations are observed in FTIR spectrum at 3222, 3086 cm^{-1} for CH_3 asymmetric stretching mode. The CH_3 symmetric stretching vibration is also observed in FTIR at 2990 cm^{-1} and in FT-Raman at 2930 cm^{-1}. The H–C–H scissoring mode of MBA is observed in FTIR at 1496, 1452 cm^{-1} and in FT-Raman at 1486 cm^{-1} with TED contribution of more than 50% (mode nos. 6–7). The weak intense bands in FTIR spectrum at 916, 872 cm^{-1} are attributed to the CH_3 rocking mode.

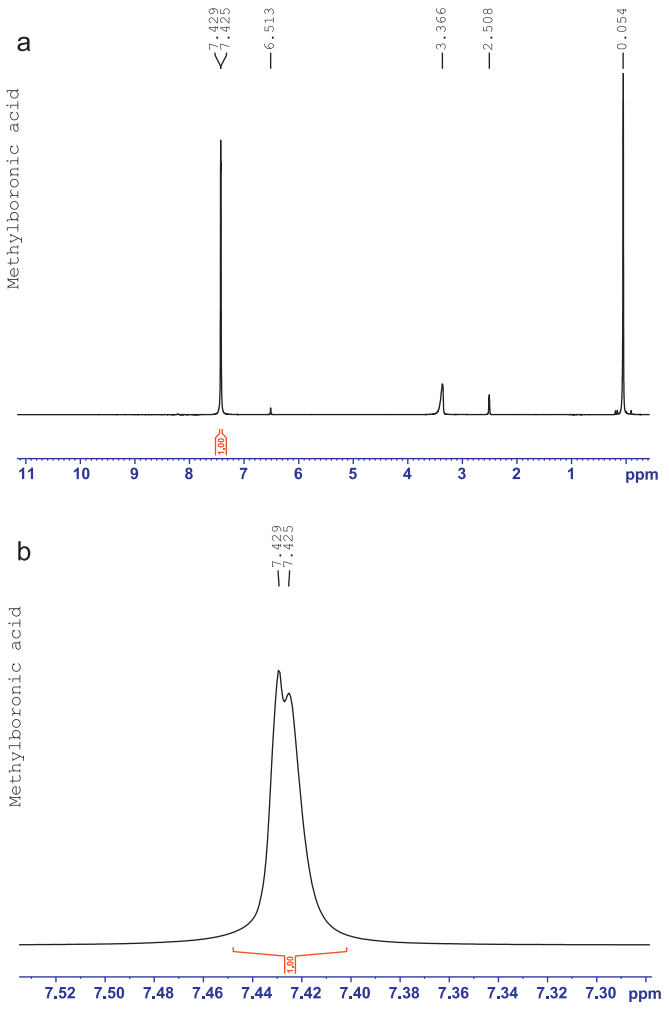

Fig. 4. (a) Proton NMR spectrum of MBA and (b) proton NMR spectrum of MBA.

6.2.2.3. $B(OH)_2$ vibrations. The B–O asymmetric stretching band of the phenylboronic acid occurs at 1370 cm^{-1} in the infrared spectrum [33] and at 1375 cm^{-1} for the phenylboronic acid linkage [38]. The corresponding bands were observed at 1402, 1380, 1244, 1172, 1004 cm^{-1} as very strong bands in FTIR and at 1359, 1187 cm^{-1} as weak bands in FT-Raman spectra of MBA molecule. These vibrations were calculated in the range 1374–988 cm^{-1} by B3LYP/6-311++G(d,p) method and in the range 1437–1058 cm^{-1} by HF method. The TED calculations show that the B–O stretching

Table 6
Experimental and calculated absorption wavelength λ (nm), excitation energies *E* (eV) and oscillator strengths (*f*) of MBA.

Experimental		TD-DFT/B3LYP/6-311++G(d,p)						Major contribution
Ethanol		Gas			Ethanol			
λ (nm)	*E* (eV)	λ (nm)	*E* (eV)	(*f*)	λ (nm)	*E* (eV)	(*f*)	
245	5.0671	166.76	7.4348	0.0007	163.34	7.5904	0.0002	Homo → Lumo (95%)

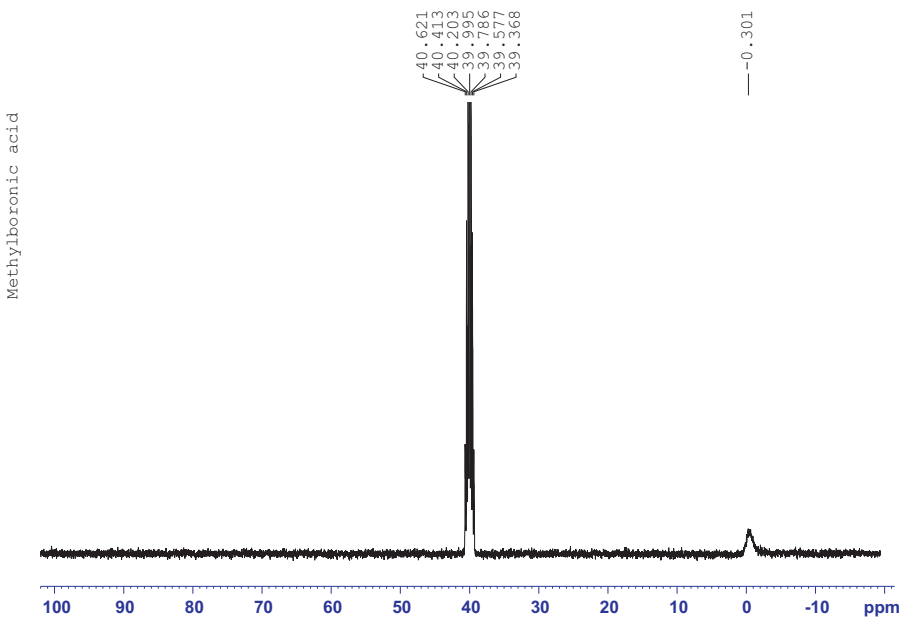

Fig. 5. Carbon NMR spectrum of MBA.

mode is a mixed mode. The computed wavenumbers are in line with the experimental wavenumbers as well as literature data [17]. The B–C stretching band was observed at 1402 cm^{-1} in FTIR for vibration of the MBA molecule. The corresponding vibration was calculated at 1374 cm^{-1} in DFT method and at 1476 cm^{-1} in HF method. The O–B–O and O–B–C in-plane bending vibrations are also predicted and compared with the experimental findings. These vibrations attained the maximum TED contribution.

6.2.3. NMR spectral analysis

The theoretical ^{1}H and ^{13}C NMR chemical shifts of MBA have been compared with the experimental data as shown in Table 5. According to these results, the calculated chemical shifts and coupling constants are in compliance with experimental findings. Chemical shifts were reported in ppm relative to TMS for ^{1}H and ^{13}C NMR spectra. Relative chemical shifts were then estimated by using the corresponding TMS shielding calculated in advance at the same theoretical level as the reference. Calculated ^{1}H isotropic chemical shielding for TMS at the HF, B3LYP/6-311++G(d,p) levels were 31.97 and 32.45 ppm respectively. Also, calculated ^{13}C isotropic chemical shielding for TMS at the HF, B3LYP/6-311++G(d,p) levels were 184.07 and 195.83 ppm, respectively. ^{1}H and ^{13}C NMR spectra are shown in Figs. 4 and 5.

The calculated proton NMR chemical shift show moderate agreement with experimental values, due to fact that free rotation of the methyl group of the molecule, the chemical shifts associated to the protons in a methyl group are mediated and thus they must be equal as shown by experimental results. The ^{13}C NMR chemical shift value is very low since MBA molecule is an inorganic acid and B3–C1 bond polarized. The calculations give different isotropic shielding because a fixed geometry was used for this purpose.

6.3. Electronic properties

6.3.1. UV absorption spectra

The major contributions of the transitions were designated with the aid of SWizard program [39]. The calculated band is predicted as $n \rightarrow \pi^*$ transition. In view of calculated absorption spectra, the absorption wavelength corresponds to the electronic transition from HOMO to LUMO with 49% for MBA molecule. The electronic absorption spectra of title molecule were measured in ethanol at room temperature. The absorption wavelength, excitation energies and oscillator strengths for the title molecule at the optimized geometry in the ground state were obtained in the framework of TD-DFT calculations with the B3LYP/6-311++G(d,p) method. It is obvious that to use TD-DFT calculations to predict the electronic absorption spectra is a quite reasonable method. The theoretical and experimental maximum absorption wavelengths are compared in Table 6. Briquet and Vercauteren reported that TD-DFT λ_{max} calculations by 6-311++G(d,p) basis set is compatible with experimental results [40]. Test calculations have shown that the inclusion of extra polarization functions does not affect the excitation energies, besides the addition of diffuse functions leads to an increase in computation time. The experimental and theoretical absorption spectra are shown in Fig. 6. The absorption wavelength values obtained with B3LYP/6-311++G(d,p) are 166.76 nm (in gas phase) and 163.34 nm (in ethanol). These calculated values have red shift with experimental value 245 nm. The reason for this red shift is solvent effect which can affect the geometry and electronic structure as well as the properties of the molecule as solvent effects induce the lower energy of the molecules, and generate more significant red shift for absorption bands [41]. Comparing the calculated values with the corresponding experimental values, TD-DFT method for both in gas phase and solvent media is useful to predict UV–vis spectrum.

6.3.2. Frontier molecular orbitals analysis

The frontier molecular orbitals are important in determining such properties as molecular reactivity and the ability of a molecule to absorb light. The frontier molecular orbitals also play an important role in the electric and optical properties, as well as in UV–vis spectra and chemical reactions [42,43]. These orbitals determine the way the molecule interacts with other species. Fig. 7 shows the distributions and energy levels of the HOMO−1, HOMO, LUMO and LUMO+1 orbitals computed at the B3LYP/6-311++G(d,p) level for the title compound. The calculated energy values are presented in Table 7. HOMO is mainly localized on the hydroxyl group and LUMO is delocalized over the entire molecule. HOMO−1 is delocalized over the entire molecule and LUMO+1 is localized on the hydroxyl group and methyl group. The value of the energy separation between the HOMO and LUMO is 0.30912 eV (in gas phase).

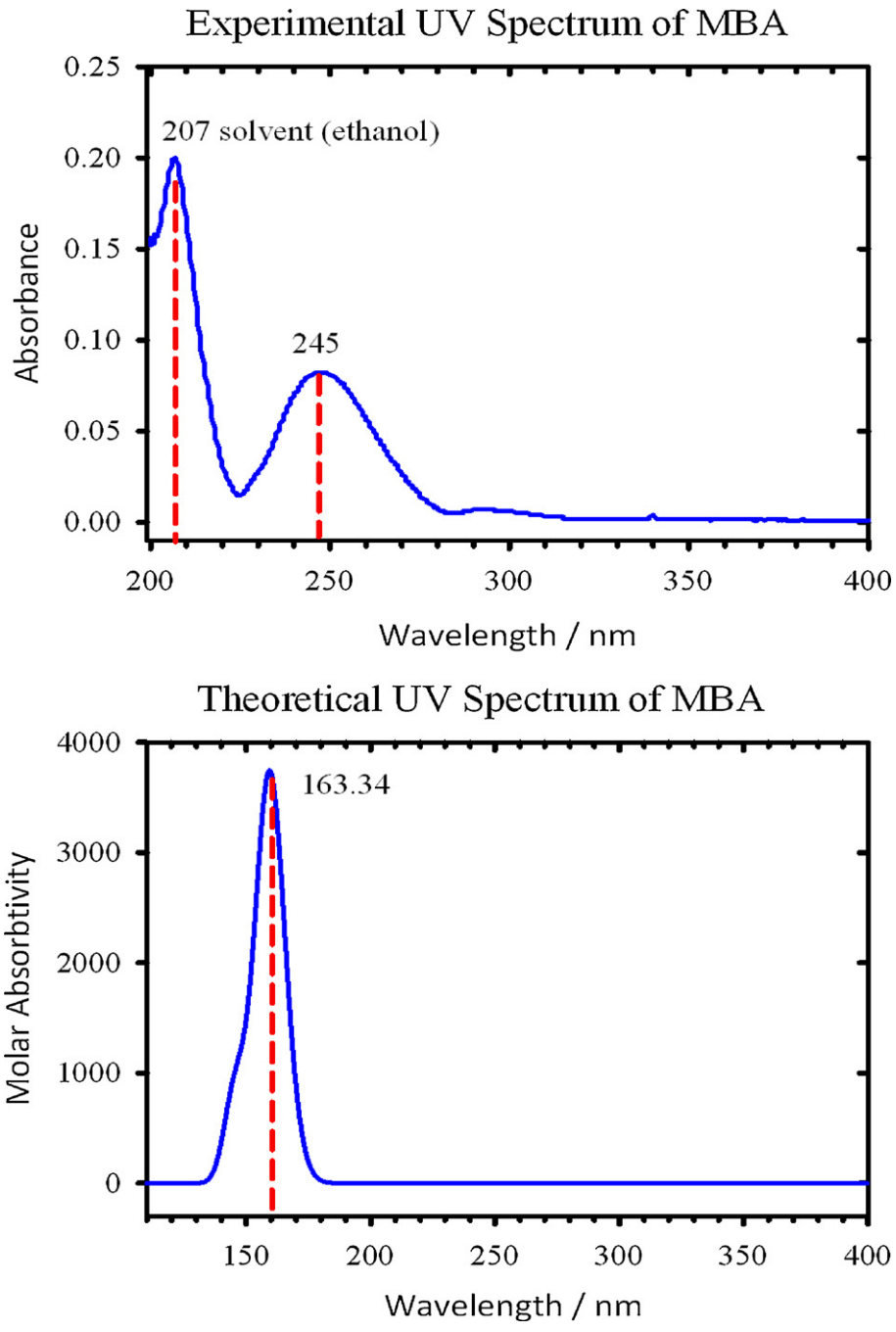

Fig. 6. Experimental and theoretical UV spectra of MBA in ethanol.

Table 7
Calculated energies values of MBA.

TD-DFT/B3LYP/6-311++G(d,p)	Gas	Ethanol
E_{total} (Hartree)	−216.61362751	−216.62994882
E_{HOMO} (eV)	−9.0914	−8.9751
E_{LUMO} (eV)	−0.5504	−0.2956
$\Delta E_{HOMO-LUMO\ gap}$ (eV)	8.5410	8.6795
E_{HOMO-1} (eV)	9.2610	−9.1085
E_{LUMO+1} (eV)	0.3217	−0.2956
$\Delta E_{HOMO-1-LUMO+1\ gap}$ (eV)	8.9393	8.8129
Dipole	1.59160	2.04580

The lowering of the HOMO–LUMO band gap is essentially a consequence of the large stabilization of the LUMO due to the strong electron-acceptor ability of the electron-acceptor group. The higher the energy of HOMO, the easier it is for HOMO to donate electrons whereas it is easier for LUMO to accept electrons when the energy of LUMO is low.

6.4. Thermodynamic properties

All the thermodynamic data provide helpful information for the study of thermodynamic energies and estimate directions of chemical reactions according to the second law of thermodynamics in thermochemical field [44]. The thermodynamic parameters such as zero-point vibrational energy, thermal energy, specific heat

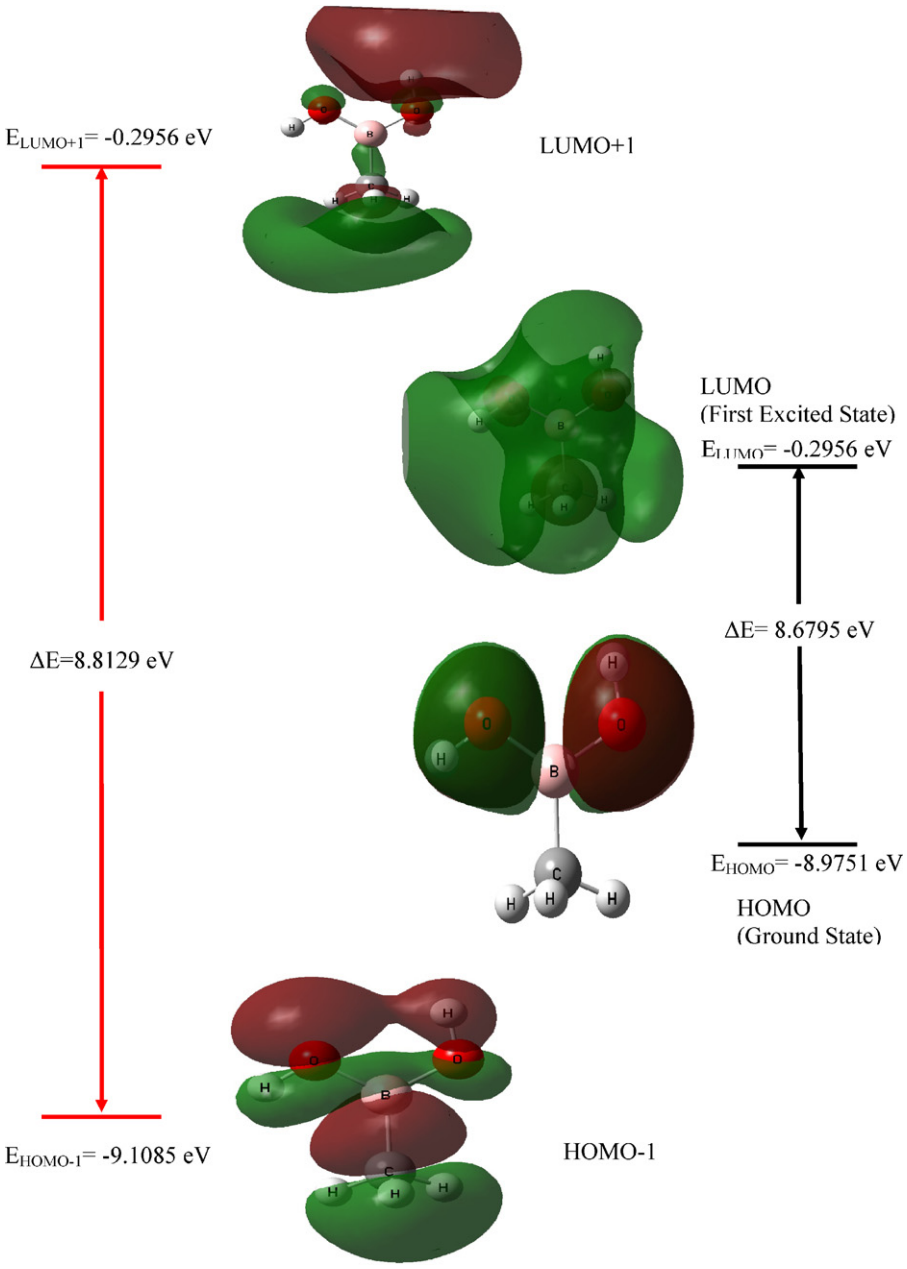

Fig. 7. The frontier and second frontier molecular orbitals of MBA in ethanol.

capacity, rotational constants, entropy, and dipole moment of MBA molecule are calculated by B3LYP method using 6-311++G(d,p) as basis set. Table 8 demonstrates several thermodynamic parameters of the title compound without of results of experimental.

Table 8
The calculated thermo dynamical parameters of MBA at 298.15 K.

Basic set	HF	B3LYP
SCF Energy (a.u)	−215.38157269	−216.61370758
Zero point vib. energy (kcal mol^{-1})	47.11989	44.22720
Rotational constants (Ghz)	9.91053	9.77074
	8.09419	8.14671
	4.55064	4.59636
Specific heat (C_v) (cal mol^{-1} K^{-1})	16.618	17.432
Entropy (S) (cal mol^{-1} K^{-1})	71.982	73.115
Dipole moment (Debye)	1.6407	1.6006

To determine thermodynamical properties of the title compound, the standard thermodynamic functions: heat capacity $C^0_{p,m}$, standard entropy S^0_m, and standard enthalpy changes ΔH^0_m based on the vibrational analysis at B3LYP/6-311++G(d,p) level were obtained and listed in Table 9. The scale factors for frequencies are 0.9050 (HF), 0.953 and 0.983 (B3LYP), which are used for an accurate prediction in determining the thermodynamic functions. As can be seen from Table 9, the thermodynamic functions are increasing with temperature ranging from 100 to 600 K due to the fact that the molecular vibrational intensities increase with temperature [45]. The correlation equations between heat capacities, entropies, enthalpy changes and temperatures were fitted by quadratic formulas, and the corresponding fitting factors (R^2) for these thermodynamic properties are 0.9957, 0.9989 and 0.9685, respectively. The correlation graphs are shown in Figs. 8–10.

Table 9
Thermodynamic properties at different temperatures at the B3LYP/6-311++G(d,p) level for MBA.

T (K)	$C^0_{p,m}$ (cal mol^{-1} K^{-1})	S^0_m (cal mol^{-1} K^{-1})	ΔH^0_m (kcal mol^{-1})
100	8.105	58.545	0.854
150	10.787	63.125	1.423
200	13.975	67.226	2.139
250	17.518	71.163	3.025
298.15	21.060	74.901	4.049
300	21.196	75.044	4.092
350	24.793	78.830	5.342
400	28.162	82.689	6.767
450	31.234	86.421	8.352
500	33.991	90.066	10.083
550	36.451	93.613	11.945
600	38.643	97.054	13.923

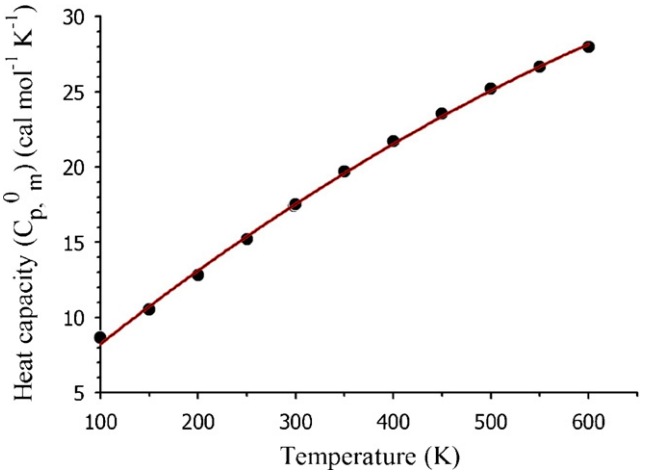

Fig. 8. Correlation graphic of heat capacity and temperature for MBA molecule.

6.5. Mulliken atomic charges

The Mulliken atomic charges are calculated by determining the electron population of each atom as defined by the basis function. The Mulliken atomic charges of MBA molecule calculated by DFT/B3LYP and HF method using 6-311++G(d,p) basis set in gas phase are shown in Table 10. Mulliken atomic charges shows that the H6 and H7 atoms have bigger positive atomic charges [0.2840e (Mulliken) for H6, 0.2613e (Mulliken) for H7 (B3LYP method)] than the other hydrogen atoms. This is due to the presence of electronegative oxygen atom, the hydrogen atoms attract the positive charge from the oxygen atoms. Oxygen atoms have the maximum negative charge value −0.4502 for O4 atom, −0.4661 for O5 atom at HF method and −0.3917 for O4 atom, −0.3919 for O5 atom at B3LYP level of calculations. The boron atom has more positive charge than the hydrogen atoms because of the substitution of oxygen atoms of the two-hydroxyl groups. Similarly, the carbon atom shows more negative charge by attracting the negative charge from the boron atom.

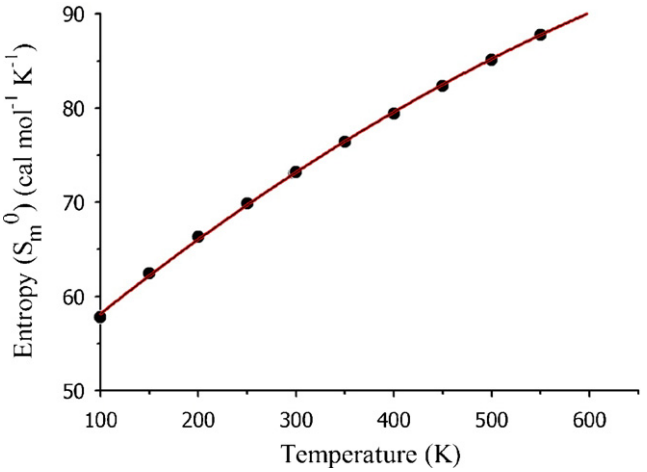

Fig. 9. Correlation graphic of entropy and temperature for MBA molecule.

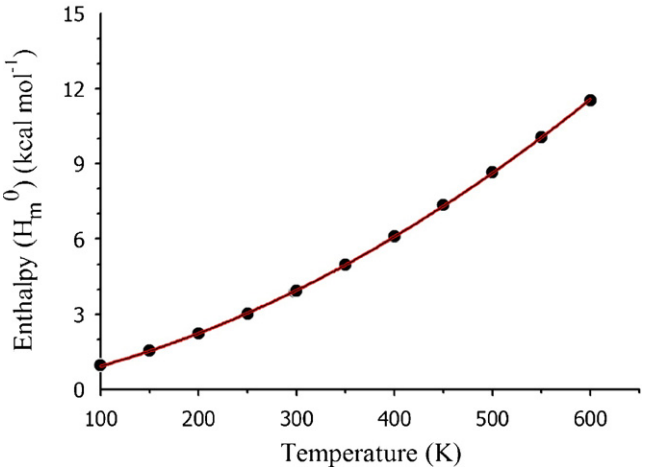

Fig. 10. Correlation graphic of enthalpy and temperature for MBA molecule.

Table 10
Mulliken charges of methylboronic acid with 6-311++G(d,p) basis set.

Atom	HF	B3LYP
C1	−0.617648	−0.601402
B3	0.556382	0.421363
O4	−0.450249	−0.391725
O5	−0.466194	−0.391903
H2	0.146657	0.156102
H6	0.306483	0.284013
H7	0.267074	0.261319
H8	0.107435	0.108216
H9	0.150059	0.154016

7. Conclusions

The title molecular structure was characterized by FTIR, FT-Raman, UV–vis, ^{1}H and ^{13}C NMR spectroscopy. The molecular structural parameters, thermodynamic properties, vibrational frequencies and chemical shifts (^{13}C and ^{1}H) of the fundamental modes of MBA optimized geometry have been determined from ab initio and DFT calculations. The geometry was optimized without any symmetry constraints using the DFT/B3LYP and HF methods with 6-311++G(d,p) basis set. DFT calculations at B3LYP/6-311++G(d,p) level for the title compound showed that the optimized geometry closely resembled the crystal structure. A comparison between calculated vibrational spectra and their experimental counterpart showed a good correlation. To fit the theoretical vibrational frequency results with experimental ones for B3LYP, we have multiplied by the scale factor 0.958, 0.983 whereas for HF method the scale factor 0.9050 was used. Gained multiplication factors results seemed to be in good agreement with experimental data. In particular, the results of B3LYP method has shown better fit to experimental data than those of HF in evaluating vibrational frequencies. The electric dipole moments and the first hyperpolarizabilities of the compound studied have been

calculated by B3LYP/6-311++G(d,p) method. Absorption maximum (λ_{max}) of MBA was calculated by TD-DFT method and compared with experimental UV–vis spectra.

Appendix A. Supplementary data

Supplementary data associated with this article can be found, in the online version, at doi:10.1016/j.saa.2012.02.036.

References

[1] W. Tjarks, A.K.M. Anisuzzaman, L. Liu, S.H. Soloway, R.F. Barth, D.J. Perkins, D.M. Adams, J. Med. Chem. 35 (1992) 16228–17861.
[2] Y. Yamamoto, Pure Appl. Chem. 63 (1991) 423–426.
[3] F. Alam, A.H. Soloway, R.F. Barth, N. Mafune, D.M. Adam, W.H. Knoth, J. Med. Chem. 32 (1989) 2326–2330.
[4] M.R. Stabile, et al., Bioorg. Med. Chem. Lett. 21 (1996) 2501–2506.
[5] P.R. Westmark, B.D. Smith, J. Pharm. Sci. 85 (1996) 266–269.
[6] N.A. Petasis, Aust. J. Chem. 60 (2007) 795–798.
[7] E. Cuthbertson, Boronic Acids: Properties and Applications, Alfa Aesar, Heysham, 2006.
[8] D.G. Hall (Ed.), Boronic Acids: Preparation, Applications in Organic Synthesis and Medicine, Wiley-VCH, Weinheim, 2005.
[9] A.H. Soloway, R.G. Fairchild, Sci. Am. 262 (1990) 100–107.
[10] D.A. Matthews, R.A. Alden, J.J. Birktoft, S.T. Freer, J. Kraut, J. Biol. Chem. 250 (1975) 7120–7126.
[11] D.H. Kinder, S.K. Frank, M.M. Ames, J. Med. Chem. 33 (1990) 819–823.
[12] L. Bobcock, R. Pizer, Inorganic Chem. 19 (1980) 56–61.
[13] O.Yu. Valiakhmetova, S.A. Bochkor, V.V. Kuznetsov, J. S. Chem. 573 (2010) 573–576.
[14] M. Kurt, J. Raman Spectrosc. 40 (2009) 67–75.
[15] P.N. Horton, M.B. Hursthouse, M.A. Becket, M.P.R. Hankey, Acta Cryst. E Struct. Rep. E 60 (2004) o2204.
[16] M. Kurt, T.R. Sertbakan, M. Özduran, M. Karabacak, J. Mol. Struct. 921 (2009) 178–187.
[17] S. Ayyappan, N. Sundaraganesan, M. Kurt, T.R. Sertbakan, M. Özduran, J. Raman Spectrosc. 41 (2010) 1379–1387.
[18] Ö. Alver, C. Parlak, Vib. Spectr. 54 (2010) 1–9.
[19] D.C. Young, Computational Chemistry: A Practical Guide for Applying Techniques to Real World Problems (Electronic), John Wiley & Sons Inc, New York, 2001.
[20] N. Sundaraganesan, S. Ilakiamani, H. Saleem, P.M. Wojciechowski, D. Michalska, Spectrohim. Acta A 61 (2005) 2995–3001.
[21] J. Baker, A.A. Jarzecki, P. Pulay, J. Phys. Chem. A 102 (1998) 1412–1424.
[22] SQM version 1.0, Scaled Quantum Mechanical Force Field, 2013 Green Acres Road, Fayetteville, Arkansas 72703.
[23] R. Ditchfield, J. Chem. Phys. 56 (1972) 5688–5691.
[24] K. Wolinski, J.F. Hinton, P. Pulay, J. Am. Chem. Soc. 112 (1990) 8251–8260.
[25] M.J. Frisch, G.W. Trucks, H.B. Schlegel, G.E. Scuseria, M.A. Robb, J.R. Cheeseman, G. Scalmani, V. Barone, B. Mennucci, G.A. Petersson, H. Nakatsuji, M. Caricato, X. Li, H.P. Hratchian, A.F. Izmaylov, J. Bloino, G. Zheng, J.L. Sonnenberg, M. Hada, M. Ehara, K. Toyota, R. Fukuda, J. Hasegawa, M. Ishida, T. Nakajima, Y. Honda, O. Kitao, H. Nakai, T. Vreven, J.A. Montgomery Jr., J.E. Peralta, F. Ogliaro, M. Bearpark, J.J. Heyd, E. Brothers, K.N. Kudin, V.N. Staroverov, R. Kobayashi, J. Normand, K. Raghavachari, A. Rendell, J.C. Burant, S.S. Iyengar, J. Tomasi, M. Cossi, N. Rega, J.M. Millam, M. Klene, J.E. Knox, J.B. Cross, V. Bakken, C. Adamo, J. Jaramillo, R. Gomperts, R.E. Stratmann, O. Yazyev, A.J. Austin, R. Cammi, C. Pomelli, J.W. Ochterski, R.L. Martin, K. Morokuma, V.G. Zakrzewski, G.A. Voth, P. Salvador, J.J. Dannenberg, S. Dapprich, A.D. Daniels, Ö. Farkas, J.B. Foresman, J.V. Ortiz, J. Cioslowski, D.J. Fox, Gaussian 09, Revision A. 1, Gaussian, Inc, Wallingford, CT, 2009.
[26] G. Keresztury, S. Holly, J. Varga, G. Besenyei, A.Y. Wang, J.R. Durig, Spectrochim. Acta 9A (1993) 2007–2026.
[27] G. Keresztury, in: J.M. Chalmers, P.R. Griffith (Eds.), Raman Spectroscopy: Theory, Hand book of Vibrational Spectroscopy, vol. 1, John Wiley & Sons Ltd, New York, 2002.
[28] C.R. Zhang, H.S. Chen, G.H. Wang, Chem. Res. Chin. U 20 (2004) 640–646.
[29] Y. Sun, X. Chen, L. Sun, X. Guo, W. Lu, Chem. Phys. Lett. 381 (2003) 397–403.
[30] O. Christiansen, J. Gauss, J.F. Stanton, Chem. Phys. Lett. 305 (1999) 147–155.
[31] G. Ambady, G. Karth, J. Cryst. Mol. Struct. 3 (1973) 37–45.
[32] S.J. Rettig, J. Trotter, Can. J. Chem. 55 (1977) 3071–3075.
[33] J.A. Faniran, H.F. Shurvell, Can. J. Chem. 46 (1968) 2089–2095.
[34] D. Sajan, I. Hubert Joe, V.S. Jayakumar, J. Zaleski, J. Mol. Struct. 785 (2006) 43–53.
[35] P.S. Kalsi, Spectroscopy of Organic Compounds, Wiley Eastern Limited, New Delhi, 1993.
[36] D. Sajan, I. Hubert Joe, V.S. Jayakumar, J. Raman Spectrosc. 37 (2005) 508–519.
[37] M. Gussoni, C. Castiglioni, M.N. Ramos, M.C. Rui, G. Zerbi, J. Mol. Struct. 224 (1990) 445–470.
[38] G. Kahraman, O. Beskarcles, Z.M. Rzave, E. Piskin, Polymer 45 (2004) 5813–5828.
[39] S.I. Gorelsky, SWizard Program Revision 4.5, University of Ottawa, Ottawa, Canada, 2010, Available from: http://www.sg.chem.net/.
[40] L. Briquet, D.P. Vercauteren, J.M. André, E.A. Perpète, D. Jacquemin, Chem. Phys. Lett. 435 (2007) 257–262.
[41] M. Snehalatha, C. Ravikumar, I. Hubert Joe, N. Sekar, V.S. Jayakumar, Spectrochim. Acta 72A (2009) 654–662.
[42] Fleming, Frontier Orbitals and Organic Chemical Reactions, Wiley, London, 1976.
[43] T. Karakurt, M. Dinçer, A. Çetin, M. Sekerci, Spectchim. Acta Part A 77 (2010) 189–198.
[44] R. Zhang, B. Dub, G. Sun, Y. Sun, Spectrochim. Acta A 75 (2010) 1115–1124.
[45] J. Bevan Ott, J. Boerio-Goates, Calculations from Statistical Thermodynamics, Academic Press, 2000.